A Remarkable Family of Rhodium Acetonitrile Compounds Spanning Three Oxidation States and with Nuclearities Ranging from Mononuclear and Dinuclear to One-Dimensional Chains

ARTICLE *in* JOURNAL OF THE AMERICAN CHEMICAL SOCIETY · AUGUST 1999

Impact Factor: 12.11 · DOI: 10.1021/ja991130e

9 AUTHORS, INCLUDING:

Laura Pence
University of Hartford
38 PUBLICATIONS **795** CITATIONS
SEE PROFILE

Charles Campana
Bruker Corporation
180 PUBLICATIONS **3,374** CITATIONS
SEE PROFILE

Kim R Dunbar
Texas A&M University
442 PUBLICATIONS **13,157** CITATIONS
SEE PROFILE

A Remarkable Family of Rhodium Acetonitrile Compounds Spanning Three Oxidation States and with Nuclearities Ranging from Mononuclear and Dinuclear to One-Dimensional Chains

M. E. Prater,[†] L. E. Pence,[†] R. Clérac,[†] G. M. Finniss,[†] C. Campana,[‡] P. Auban-Senzier,[§] D. Jérome,[§] E. Canadell,[||] and K. R. Dunbar*,[†]

Contribution from the Department of Chemistry and The Center for Fundamental Materials Research, Michigan State University, East Lansing, Michigan 48824 , Bruker, Madison, WI, Laboratoire de Physique des Solides, URA 02, Bat 510 Université Paris-Sud Orsay Cedex, 91405 France, and Institut de Ciencia de Materials de Barcelona (CISC), Campus de la UAB, E-08193 Bellaterra, Spain

Received April 9, 1999

Abstract: A series of homoleptic cations of Rh(I,II), Rh(II), and Rh(III) have been synthesized and characterized in the solid-state and in solution. Three new dinuclear compounds of dirhodium(II,II) were prepared by treatment of $Rh_2(O_2CCH_3)_4(L)_2$ with Et_3OBF_4 or $Me_3Si(CF_3SO_3)$ in acetonitrile or propionitrile. The cations in $[Rh_2^{II,II}(MeCN)_{10}][BF_4]_4$ (**1**), $[Rh_2^{II,II}(MeCN)_{10}][SO_3CF_3]_4$ (**2**), and $[Rh_2^{II,II}(EtCN)_{10}][BF_4]_4$ (**3**) contain eight equatorial RCN groups oriented in an approximately square planar arrangement around the two Rh atoms and two axial RCN molecules. The redox properties of **1**−**3** were investigated by cyclic voltammetry, which revealed the presence of one or two irreversible reduction(s) but no oxidations. Although there was no electrochemical evidence for an accessible oxidation, it was found that treatment of $[Rh_2^{II,II}(MeCN)_{10}][BF_4]_4$ with $NOBF_4$ occurs to yield another member of the homoleptic acetonitrile family, namely, the octahedral d^6 cation $[Rh^{III}(MeCN)_6][BF_4]_3$, (**4**). The corresponding one-electron reduction product was isolated by a slow galvanostatic reduction of $[Rh_2^{II,II}(MeCN)_{10}][BF_4]_4$ (**1**) in MeCN at a Pt electrode. The crystals harvested from the cathode were found to be the unprecedented mixed-valence 1-D chain compound $[Rh^{I,II}(MeCN)_4(BF_4)_{1.5}]_x$ (**5**), which result from a radical polymerization of the unstable $Rh_2^{I,II}$ dinuclear cation. In an effort to access the final member of this series, namely, the homoleptic Rh^I species, the dicarbonyl compound $[Rh^I(CO)_2(MeCN)_2][BF_4]$ (**6**) was prepared, but all thermal and photochemical attempts to remove the CO ligands led to the conclusion that only one CO is labile. The mixed-ligand, square planar cation $[Rh^I(CO)_2(MeCN)_2]^+$ was found to form a 1-D stack in the solid state, unlike previously reported salts with bulky counterions. For all of the compounds under investigation, infrared spectroscopy and X-ray studies were performed. The mixed-valence product was also characterized by EPR spectroscopy and SQUID magnetometry.

I. Introduction

One of our current research interests is the use of fully solvated transition metal species as building blocks in molecule-based materials. The advantage of these starting materials is that they contain labile ligands which are neither electronically nor sterically demanding, a situation that allows for deliberate introduction of the dirhodium unit into a variety of ligand environments under mild conditions. Mononuclear compounds stabilized solely by solvent ligands are common, especially for 3d metals,[1] but until fairly recently, the only documented dinuclear analogues were the aqueous cations $Rh_2(aq)^{4+}$ and $Mo_2(aq)^{4+}$ prepared in strong acid media.[2] To avoid the difficulties of an acidic medium, we and others have employed an alternate method to access solvated species, namely, alkylation of the acetate ligands in $M_2(O_2CCH_3)_4$ compounds with triethyloxonium tetrafluoroborate. This strategy was reported by several groups to produce the partially substituted compounds *cis*-$[M_2(O_2CCH_3)_2(MeCN)_2]^{2+}$ (M = Mo, Rh),[3,4] but attempts to access the homoleptic acetonitrile cations by this route were not made at this time. We later demonstrated that $Rh_2(O_2CCH_3)_4(MeOH)_2$ treated with an excess of Et_3OBF_4 or HBF_4 in refluxing acetonitrile yields the remarkably stable, unbridged cation $[Rh_2(MeCN)_{10}]^{4+}$ with a single Rh−Rh bond.[5] These approaches have also proven to be successful for the synthesis of the quadruply bonded $[Mo_2(MeCN)_{8-10}]^{4+}$ species from $Mo_2(O_2CCH_3)_4$.[6] A further extension of the dinuclear homoleptic acetonitrile series to include the triply bonded $[Re_2(MeCN)_{10}]^{4+}$

* To whom correspondence should be addressed. E-mail: dunbar@mail.chem.tamu.edu.

[†] Michigan State University.

[‡] Bruker.

[§] Université Paris-Sud Orsay Cedex.

[||] Institut de Ciencia de Materials de Barcelona (CISC).

(1) (a) Hathaway, B. J.; Holah, D. G.; Underhill, A. E. *J. Chem. Soc.* **1962**, 2444. (b) Zuur, A. P.; van Houte, J. J.; Groeneveld, W. L. *Recl. Trav. Chim. Pays-Bas* **1968**, *87*, 755. (c) Driessen, W. L.; Groeneveld, W. L. *Recl. Trav. Chim. Pays-Bas* **1969**, *88*, 977. (d) Habeeb, J. J.; Said, F. F.; Tuck, D. G. *J. Chem. Soc., Dalton Trans.* **1981**, 118. (e) Driessen, W. L.; Reedijk, J. *Inorg. Synth.* **1992**, *29*, 111. (f) Buschmann, W. E.; Miller, J. S. *Chem. Eur. J.* **1998**, *4*, 1731. (g) Heintz, R. A.; Smith, J. A.; Szalay, P. S.; Weisgerber, A.; Dunbar, K. R. *Inorg. Synth.*, in press.

(2) (a) Maspero, F.; Taube, H. *J. Am. Chem. Soc.* **1968**, *90*, 7361. (b) Ziólkowski, J. J.; Taube, H. *Bull. Acad. Pol. Sci.* **1973**, *21*, 113. (c) Bowen, A. R.; Taube, H. *Inorg. Chem.* **1974**, *13*, 2245.

(3) (a) Pimblett, G.; Garner, C. D.; Clegg, W. *J. Chem. Soc., Dalton Trans.* **1986**, 1257. (b) Cotton, F. A.; Reid, A. H.; Schwotzer, W. *Inorg. Chem.* **1985**, *24*, 3965.

(4) Casas, J. M.; Cayton, R. H.; Chisholm, M. H. *Inorg. Chem.* **1991**, *30*, 358.

(5) Dunbar, K. R. *J. Am. Chem. Soc*. **1988**, *110*, 8247.

10.1021/ja991130e CCC: $18.00
Published on Web 08/18/1999

derivative was carried out in our laboratories by reacting $Re_2Cl_4(P\text{-}n\text{-}Pr_3)_4$ with HBF_4 in CH_3CN,[7] a method that was later found to be applicable to the synthesis of the Tc derivative.[8] Routes involving the use of trifluoromethanesulfonic acid have also been used to prepare the Mo_2^{4+} and Rh_2^{4+} acetonitrile species,[9] as well as the first homoleptic M−M bonded cation with ammonia ligands, $[Mo_2(NH_3)_8][TFMS]_4$.[10]

The purpose of the present work is to report a number of important developments in the coordination chemistry of rhodium cations with acetonitrile as the sole supporting ligand and the further characterization of a possible precursor for the currently unknown Rh^I acetonitrile cation. We have known for some time that the Rh−Rh single bond in $[Rh_2(MeCN)_{10}][BF_4]_4$ is surprisingly robust in the presence of a variety of ligands,[11] a fact that led to an investigation as to whether the mononuclear $[Rh^I(MeCN)_4][BF_4]$ and $[Rh^{III}(MeCN)_6][BF_4]_3$ species are actually stable with respect to the dinuclear $Rh^{II}-Rh^{II}$ compound.[12] A detailed photochemical study revealed that the formation of Rh^{II} radicals as well as Rh^I and Rh^{III} species occurs upon irradiation of $[Rh_2(MeCN)_{10}][BF_4]_4$ in MeCN but that, within the time scale of 1 h, the dinuclear cation is regenerated in essentially quantitative yields![13] To understand the unusually high stability of the homoleptic dinuclear $Rh_2^{II,II}$ compound, we have now prepared the one-electron oxidized and reduced forms and studied their solution and solid-state properties. Herein we report the syntheses and full characterization of an unprecedented series of acetonitrile compounds in formal oxidation states of Rh^I, Rh^{II}, Rh^{III}, and $Rh^{I/II}$ that exhibit remarkable structural diversity. For three of the four members of these series (Rh^{II}, Rh^{III}, $Rh^{I/II}$), the nuclearities range from mononuclear and dinuclear to polymeric metal−metal bonded chains with the ligands being only acetonitrile in all cases. A portion of this work has appeared in preliminary communication form.[5,14]

II. Experimental Section

A. Starting Materials. Unless otherwise stated, all manipulations were performed at room temperature under anaerobic conditions with standard vacuum line and Schlenk techniques. Triethyloxonium tetrafluoroborate in dichloromethane, tetrafluoroboric acid/diethyl ether, nitrosonium tetrafluoroborate, and trimethylsilyltriflate were obtained from Aldrich and purged with dinitrogen prior to use. All solvents, with the exception of water and acetonitrile, were dried by conventional methods and freshly distilled before use. Acetonitrile was distilled under nitrogen over 3 Å molecular sieves, passed down an activated alumina column, and stored under a nitrogen atmosphere until use. Sodium acetate was purchased from Aldrich and was used without further purification. Tetrabutylammonium tetrafluoroborate was obtained from Aldrich and recrystallized from ethyl acetate before use. $Rh_2(OAc)_4(MeOH)_2$ was purchased from Sigma as the bis-aqua adduct or prepared from $RhCl_3 \cdot xH_2O$ according to the established literature procedure.[15] $Rh_2(O_2CCF_3)_4$ was obtained from Pressure Chemical Co. and used without further purification. $Rh_2(OAc)_4(H_2O)_2$ was converted to $Rh_2(OAc)_4(MeOH)_2$ by recrystallization from MeOH. Conversion to $Rh_2(OAc)_4(MeCN)_2$ is achieved by recrystallizing $Rh_2(OAc)_4(MeOH)_2$ from MeCN.

B. Preparation of $[Rh_2^{II,II}(MeCN)_{10}][BF_4]_4$ (1). 1. From $Rh_2(O_2CCF_3)_4$ and Et_3OBF_4. In a standard reaction, 0.621 g (0.9438 mmol) of $Rh_2(O_2CCF_3)_4$ was placed in a 100 mL pear-shaped flask equipped with a stirbar and a reflux condenser. Acetonitrile (30 mL) and 1 M triethyloxonium tetrafluoroborate in CH_2Cl_2 (13 mL) were added to the flask, and the resulting purple solution was allowed to reflux for 5 days under a nitrogen atmosphere. The volume of the orange solution was reduced to ~10 mL, and CH_2Cl_2 (60 mL) was added to precipitate the product. The orange solid was washed with 10 mL of dichloromethane and 2 × 10 mL of Et_2O. The reaction yielded 0.657 g (0.6812 mmol) of $[Rh_2(MeCN)_{10}][BF_4]_4$ (72% yield). The product is recrystallized by layering a saturated acetonitrile solution of the product with dichloromethane. The solid is hygroscopic as evidenced by its facile conversion to the pink axial bis-water adduct when exposed to humid laboratory air. The salt is soluble in MeCN, H_2O, DMSO, and CH_3NO_2 but is insoluble in THF, alcohols, acetone, and CH_2Cl_2. Anal. calcd for $C_{20}H_{30}B_4F_{16}N_{10}Rh_2$: C, 24.93; H, 3.14; F, 31.55. Found: C, 25.44; H, 3.58; F, 31.37. IR (CsI, Nujol), cm^{-1}: 2342 (m), 2317 (m), 2300 (w), 1062 (vs, br), 1024 (vs, br). ^1H NMR (CD_3CN, anaerobic): $\delta =$ 2.65 (s, equatorial CH_3CN), 1.95 (s, free CH_3CN). UV−Vis (MeCN, anaerobic): λ_{max}, nm (ϵ in $M^{-1}cm^{-1}$) = 468 (570), 277 (24 400). The use of $Rh_2(O_2CCF_3)_4$ is more convenient than beginning with $Rh_2(OAc)_4(MeOH)_2$, as the trifluoroacetate groups are more labile which leads to shorter reaction times.[16]

2. From $Rh_2(O_2CCH_3)_4$ and HBF_4. In a typical reaction, a mixture of $Rh_2(OAc)_4(MeOH)_2$ (0.200 g, 0.395 mmol), 10 mL of MeCN, and 1 mL of $HBF_4 \cdot Et_2O$ complex in diethyl ether (excess) was refluxed for 10 days. After ~7 days, an additional quantity of $HBF_4 \cdot Et_2O$ complex (0.7 mL) was added to ensure complete reaction. The initial dark purple solution gradually changed to a reddish orange color and finally to orange over the course of the reaction. (If the solution remains red, more $HBF_4 \cdot Et_2O$ should be added.) The reaction solution was allowed to cool, after which time it was layered with hexanes (1 mL) and diethyl ether (10 mL) to precipitate the product. The diethyl ether diffuses into the hexanes, and the resulting mixture is miscible with MeCN, such that complete diffusion occurs with the production of large rod-shaped orange crystals. If brown or black solids are present, the solid should be recrystallized a second time from acetonitrile/hexanes/diethyl ether. Typical yields after recrystallization are 60−70% (0.23−0.27 g). The product was characterized as reported in (i) above.

C. Preparation of $[Rh_2^{II,II}(MeCN)_{10}][TFMS]_4$ (2). An amount of $Rh_2(OAc)_4(MeCN)_2$ (0.100 g, 0.191 mmol) was dissolved in 10 mL of MeCN, treated with 0.5 mL of $Me_3Si(TFMS)$, and refluxed for 14 days. After about one week, an additional amount of $Me_3Si(TFMS)$ (0.5 mL) was added to drive the reaction to completion. The red−orange solution was layered with hexanes (1 mL) and diethyl ether (10 mL) to produce 0.163 g (73% yield) of a crystalline product. The solution was decanted, and the crystals were washed with dichloromethane followed by diethyl ether (2 × 5 mL each). The solid was dried by passing nitrogen gas over the solid. Application of a dynamic vacuum led to a loss of crystallinity and conversion of the orange product to a purple solid with axial coordination of $CF_3SO_3^-$ anions. This loss of axial acetonitrile ligands hampers attempts to obtain a reliable elemental analysis. Orange product: ($[Rh_2(MeCN)_{10}][TFMS]_4$). IR (CsI, Nujol), cm^{-1}: 2345 (s), 2316 (s), 2286 (m), 1263 (vs), 1227 (vs), 1157 (s), 1030 (s), 756 (m), 640 (vs), 572 (m), 518 (vs). ^1H NMR (CD_3NO_2): $\delta =$ 2.79 (s, 6H, equatorial CH_3CN), 2.02 (s, 1H, free CH_3CN). Integration is imprecise due to the breadth of the second resonance. Purple product. IR (CsI, Nujol), cm^{-1}: 2341 (m), 2316 (w), 1309 (m, split), 1267(s), 1228 (s),

(6) (a) Cotton, F. A.; Wiesinger, K. J.; *Inorg. Chem.* **1991**, *30*, 871. (b) Cotton, F. A.; Wiesinger, K. J. *Inorg. Synth.* **1992**, *29*, 134.
(7) (a) Bernstein, S. N.; Dunbar, K. R. *Angew. Chem., Int. Ed. Engl.* **1992**, *31*, 1360. (b) Bartley, S. L.; Bernstein, S. N.; Dunbar, K. R. *Inorg. Chim. Acta* **1993**, *213*, 213.
(8) Bryan, J. C.; Cotton, F. A.; Daniels, L. M.; Haefner, S. C.; Sattelberger, A. P. *Inorg. Chem.* **1995**, *34*, 1875.
(9) (a) Mayer, J. M.; Abbott, E. H. *Inorg. Chem.* **1983**, *22*, 2774. (b) Baranovskii, I. B.; Golubnichaya, M. A.; Zhilyaev, A. N.; Shchelokov, R. N. *Soviet J. Coord. Chem.* **1988**, *13*, 369. (c) Baranovskii, I. B.; Zhilyaev, A. N.; Dikareva, L. M. *Russ. J. Inorg. Chem.* **1988**, *33*, 1802. (d) Dikareva, L. M.; Andrianov, V. I.; Zhilyaev, A. N.; Baranovskii, I. B. *Russ. J. Inorg. Chem.* **1989**, *34*, 240.
(10) Comrie, A. G.; McVitie, A.; Peacock, R. D. *Polyhedron* **1994**, *13*, 193.
(11) Pence, L. E., Ph.D. Dissertation, Michigan State University, 1992.
(12) (a) Dunbar, K. R.; Haefner, S. C.; Pence, L. E. *J. Am. Chem. Soc.* **1989**, *111*, 5504. (b) Haefner, S. C.; Dunbar, K. R.; Bender, C. *J. Am. Chem. Soc.* **1991**, *113*, 9540.
(13) James, C. A.; Morris, D. E.; Doorn, S. K.; Arrington, C. A.; Dunbar, K. R.; Finniss, G. M.; Pence, L. E.; Woodruff, W. H. *Inorg. Chim. Acta* **1996**, *242*, 91.
(14) Finniss, G. M.; Canadell, E.; Campana, C.; Dunbar, K. R. *Angew. Chem., Int. Ed. Engl.* **1996**, *35*, 2772.
(15) Rempel, G. A.; Legzdins, P.; Smith, H.; Wilkinson, G. *Inorg. Synth.* **1972**, *13*, 90.
(16) Dunbar, K. R.; Pence, L. E. *Inorg. Synth.* **1992**, *29*, 182.

Table 1. Crystallographic Data for Compounds **1**−**6**[a]

compounds	**1**	**2**	**3**	**4**	**5**	**6**
formula	$Rh_2N_{10}C_{20}H_{30}B_4F_{16}$	$Rh_2N_{10}C_{24}H_{30}F_{12}O_{12}S_4$	$Rh_2N_{10}C_{30}H_{50}B_4F_{16}$	$RhN_6C_{12}H_{18}B_3F_{12}$	$RhN_4C_8H_{12}B_{1.5}F_6$	$RhN_2C_6H_6F_4O_2B$
form. weight	963.41	1212.48	1103.82	609.52	397.26	327.80
temp. (K)	296 ± 1	183 ± 2	183 ± 2	173 ± 2	173 ± 2	173 ± 2
space group	*C*2/*c*	*P*2$_1$/*n*	*C*2/*c*	*Pnma*	*P*6$_2$22	*C*2/*c*
a, Å	18.123(2)	12.192(6)	19.920(4)	13.866(7)	12.1121(5)	15.804(3)
b, Å	11.920(2)	22.75(1)	12.646(2)	14.128(4)	12.1121(5)	13.505(3)
c, Å	18.243(2)	18.690(8)	18.646(2)	11.877(4)	17.3157(10)	12.615(3)
α, deg	90.00	90.00	90.00	90.00	90.00	90.00
β, deg.	99.58(1)	97.52(4)	92.55(2)	90.00	120.00	122.60(3)
γ, deg	90.00	90.00	90.00	90.00	90.00	90.00
V, Å^3	3886(2)	5139(8)	4658(1)	2329(2)	2199.9(2)	2268.4(8)
Z	4	4	4	4	6	8
μ (mm^{-1})	0.9383	0.887	0.793	0.826	1.224	1.545
d_{calc}, g/cm^3	1.647	1.616	1.574	1.739	1.800	1.616
radiation	MoKα graphite monochromated (λ_α = 0.71073 Å)					
total data	2802	7354	4326	2355	11845	3527
unique data	2395	6977	3353	1621	1625	1584
*R*1	0.0520	0.075	0.047	0.028	0.0479	0.0662
wR[b] or *wR2*[c]	0.0807[b]	0.091[b]	0.072[b]	0.035[b]	0.0786[c]	0.1608[c]
GooF[d]	2.33	2.34	2.27	1.39	1.185	0.887

[a] $R1 = \Sigma\ ||F_o| - |F_c||/\Sigma\ |F_o|$. [b] $wR = [\Sigma\ w(|F_o| - |F_c|)^2/\Sigma\ wF_o^2]^{1/2}$; $w = 1/\sigma^2$. [c] $wR2 = [\Sigma\ w(F_o^2 - F_c^2)^2/\Sigma\ w(F_o^2)^2]^{1/2}$. [d] GooF $= [\Sigma\ w(|F_o| - |F_c|)^2/(N_{obs} - N_{parameters})]^{1/2}$.

1205 (s), 1157 (m), 1032 (s), 1018 (m), 1008 (s), 640 (s), 572 (w), 518 (m). ^{1}H NMR (CD_3NO_2): δ = 2.79 (s, equatorial CH_3CN).

D. Preparation of $[Rh_2^{II,II}(EtCN)_{10}][BF_4]_4$ (3). A mixture of $Rh_2(OAc)_4(MeCN)_2$ (0.205 g, 0.391 mmol), 10 mL of propionitrile, and excess (1 mL) $HBF_4{\cdot}Et_2O$ was refluxed for 2 days, during which time the solution changed from purple to a bright red−orange. The solution was allowed to cool, whereupon hexanes (1 mL) and diethyl ether (10 mL) were carefully layered on top and allowed to slowly diffuse. After 3 days, a batch of large crystals was separated from an oily solution and washed with 3 × 5 mL portions of a 1:1 diethyl ether/propionitrile mixture to remove the oily residue. The washings were added to the decanted solution, the volume was reduced under vacuum, and fresh propionitrile (5 mL) was added to dissolve the oil. Finally hexanes (1 mL) and diethyl ether (10 mL) were added to precipitate additional product. This procedure was repeated until there was a negligible quantity of dark-orange oil: combined yield, 0.290 g (67%). The lability of the axial propionitrile ligands in addition to the oily nature of **3** limited the accuracy of elemental analysis. Anal. calcd for $C_{30}H_{50}B_4F_{16}N_{10}Rh_2$: C, 32.64; H, 4.57; N, 12.69. Found: C, 31.08; H, 4.56; N, 12.07. IR (CsI, Nujol), cm^{-1}: 2324 (s), 2287 (m), 1315 (w), 1285 (w), 1055 (vs, br), 783 (m), 561 (w), 521 (m). ^{1}H NMR (CD_3CN, anaerobic): δ = 3.03 (q, 8H, equatorial-CH_3CH_2CN), 2.35 (q, 2H, free CH_3CH_2CN), 1.36 (t, 12H, equatorial-CH_3CH_2CN), 1.19 (t, 3H, free CH_3CH_2CN).

E. Preparation of $[Rh^{III}(MeCN)_6][BF_4]_3$ (4). In a typical reaction, a 0.162 g (0.168 mmol) quantity of $[Rh_2(MeCN)_{10}][BF_4]_4$ was dissolved in 20 mL of acetonitrile, $NOBF_4$ (0.079 g, 0.671 mmol) was added, and the mixture was stirred for 30 min. During this period, the color of the solution changed from orange to yellow. The solution volume was reduced to ∼5 mL, and 40 mL of CH_2Cl_2 was added to the precipitate of a pale yellow compound. Yield: 0.067 g (33% yield). IR (Nujol, KBr), cm^{-1}: 2317 (s), 1065 (s, br). ^{1}H NMR: 2.76 (s). Anal. calcd for $C_{12}H_{18}B_3F_{12}N_6Rh_1$: C, 23.64; H, 2.98; N, 13.79. Found: C, 23.68; H, 3.06; N, 12.59.

F. Preparation of Crystals of $[Rh(MeCN)_4(BF_4)_{1.5}]_x$ (5). Electrochemical reduction of $[Rh_2(MeCN)_{10}][BF_4]_4$ can be carried out in bulk at a Pt gauze electrode or by slow reaction at a Pt electrode.[13,14] The best yields of large single crystals have been obtained with ∼0.060 g of $[Rh_2(MeCN)_{10}][BF_4]_4$ in the working (cathodic) compartment and 0.2 g of $[(n\text{-}C_4H_9)_4N][BF_4]$ electrolyte in the anodic compartment of a two-compartment electrolysis cell filled with 20 mL of acetonitrile. A current of 2 μA was applied to cell, and the light orange solution in the cathodic compartment gradually turned dark red−brown with concomitant deposition of crystals on the electrode. Yields for this preparation are ∼30%. It is important to note that the electrode size and shape greatly influence the rate of crystallization and crystal size. Electrodes prepared with 24 gauge platinum wire that has been flattened to a thin wafer provide the largest crystals after a period of 3 weeks. These conditions lead to a consumption of ∼80% of the starting material. Anal. calcd for $C_{16}H_{24}B_3F_{12}N_8Rh_2$: C, 24.18; H, 3.04; N, 14.10. Found: C, 24.42; H, 3.02; N, 12.55.

G. Physical Measurements. Infrared spectra were recorded as Nujol mulls between CsI or KBr plates with a Nicolet 740 FT-IR spectrophotometer. Electronic absorption spectra were recorded on a Hitachi U-2000 or a Cary 17 spectrophotometer. Electrochemical measurements were carried out by using an EG&G Princeton applied research model 362 scanning potentiostat in conjunction with a BAS model RXY recorder. Cyclic voltammetry was performed at 22 ± 2 °C in acetonitrile or propionitrile solutions containing 0.2 M tetra-*n*-butylammoniun tetrafluoroborate ($TBABF_4$) as supporting electrolyte. $E_{1/2}$ values, determined as $(E_{p,a} + E_{p,c})/2$, were referenced to the Ag/AgCl electrode and are uncorrected for junction potentials. ^{1}H NMR experiments were carried out on a Varian Gemini-300 or a Varian VXR-300 spectrometer. Elemental analyses were performed by Galbraith Laboratories or Desert Analytics. EPR experiments were performed on a Bruker ESP300E spectrometer equipped with a ESR900 cryostat (4.2−300 K) from Oxford Instruments. Magnetic measurements were obtained on polycrystalline samples with the use of a Quantum Design, model MPMSR-2 SQUID susceptometer.

1. Computational Details. The tight-binding band structure calculations use an extended Hückel-type Hamiltonian[17] and a modified Wolfsberg−Helmholz formula to evaluate the nondiagonal H_{ij} values.[18] The exponents and parameters used were taken from ref 19.

2. X-ray Structure Determination. The structures of **1**−**6** were determined by using general procedures described elsewhere.[20,21] Pertinent crystal data are summarized in Table 1. Selected bond distances and angles are presented in Table 2.

a. $[Rh_2(MeCN)_{10}][BF_4]_4$ (1). An orange block-shaped crystal of approximate size 0.75 × 0.78 × 0.80 mm^3 was mounted with epoxy cement on the end of a glass fiber. The crystal was examined on a Nicolet P3/F diffractometer with graphite monochromated Mo Kα (λ_α = 0.71073 Å) radiation. The unit cell was determined by 25 reflections

(17) Hoffmann, R *J. Chem. Phys.* **1963**, *39*, 1397.
(18) Ammeter, J.; Bürgi, H.-B.; Thibeault, J.; Hoffmann, R. *J. Am. Chem. Soc.* **1978**, *100*, 3686.
(19) Summerville, R. H.; Hoffmann, R. *J. Am. Chem. Soc.* **1976**, *98*, 7240.
(20) Calculations were performed on a Silicon Graphics Indigo workstation, VAXSTATION 4000 computer or a VAX 11/780 computer at the Department of Chemistry, Michigan State University, East Lansing, MI, with the SHELXTL 5.0, the VAX-SDP software package or the TEXSAN software package.
(21) (a) Bino, A.; Cotton, F. A.; Fanwick, P. E. *Inorg. Chem.* **1979**, *18*, 3558. (b) Cotton, F. A.; Frenz, B. A.; Deganello, G.; Shaver, A. *J. Organomet. Chem.* **1973**, *50*, 227. (c) North, A. C. T.; Phillips, D. C.; Matthews, F. S. *Acta Crystallogr., Sect. A* **1968**, *24*, 351.

Table 2. Selected Bond Distances (Å) and Angles (deg) for Compounds **1**−**6**

	$[Rh_2(MeCN)_{10}][BF_4]_4$ (**1**)		
Rh(1)−Rh(1)′	2.624(1)	Rh(1)′−Rh(1)−N(1)	90.2(1)
Rh(1)−N(1)	1.986(4)	Rh(1)′−Rh(1)−N(5)	178.1(1)
Rh(1)−N(2)	1.980(4)	Rh(1)−N(1)−C(1)	176.2(4)
Rh(1)−N(3)	1.995(4)	N(1)−C(1)−C(2)	177.1(5)
Rh(1)−N(4)	1.985(4)	Rh(1)−N(5)−C(9)	166.1(5)
Rh(1)−N(5)	2.191(5)	N(5)−C(9)−C(10)	178.4(7)
N(1)−C(1)	1.131(5)		
N(2)−C(3)	1.159(6)		
C(1)−C(2)	1.460(7)		
C(9)−C(10)	1.437(10)		
	$[Rh_2(EtCN)_{10}][BF_4]_4$ (**3**)		
Rh(1)−Rh(1)′	2.6040(9)	Rh(1)′−Rh(1)−N(1)	91.2(1)
Rh(1)−N(1)	1.991(4)	Rh(1)′−Rh(1)−N(5)	176.9(2)
Rh(1)−N(2)	1.977(4)	Rh(1)−N(1)−C(1)	171.9(4)
Rh(1)−N(3)	1.982(4)	N(1)−C(1)−C(2)	178.5(6)
Rh(1)−N(4)	1.987(4)	Rh(1)−N(5)−C(13)	157.4(6)
Rh(1)−N(5)	2.180(6)	N(5)−C(13)−C(14)	177.7(9)
N(1)−C(1)	1.128(7)		
N(2)−C(4)	1.122(8)		
N(5)−C(13)	1.148(9)		
C(1)−C(2)	1.460(8)		
C(13)−C(14)	1.54(1)		
C(14)−C(15)	1.43(1)		
	$[Rh(MeCN)_4(BF_4)_{1.5}]_x$ (**5**)		
Rh(1)−Rh(1A)	2.9277(8)	N(1)−Rh(1)−N(2)	91.2(2)
Rh(1)−Rh(1B)	2.8442(8)	N(1)−Rh(1)−N(2A)	88.7(2)
Rh(1)−N(1)	1.991(4)	N(1)−Rh(1)−N(1A)	176.9(2)
Rh(1)−N(2)	1.985(4)	N(2)−Rh(1)−Rh(2A)	177.8(2)
		N(1)−Rh(1)−Rh(1A)	88.91(11)
		N(2)−Rh(1)−Rh(1B)	91.09(11)
		N(2)−Rh(1)−Rh(1A)	88.44(11)
		N(2)−Rh(1)−Rh(1B)	91.56(11)
	$[Rh_2(MeCN)_{10}][O_3SCF_3]_4$ (**2**)		
Rh(1)−Rh(2)	2.616(2)	C(19)−C(20)	1.53(7)
Rh(1)−N(6)	2.01(1)	C(3)−C(4)	1.51(3)
Rh(1)−N(8)	1.97(1)	C(7)−C(8)	1.48(7)
Rh(1)−N(10)	2.15(1)	C(9)−C(10)	1.56(3)
Rh(2)−N(2)	1.96(1)	C(15)−C(16)	1.48(2)
Rh(2)−N(4)	2.03(1)		
Rh(2)−N(5)	2.14(1)		
N(6)−C(11)	1.10(2)	Rh(1)−N(6)−C(11)	176(1)
N(8)−C(15)	1.15(2)	Rh(1)−N(10)−C(19)	174(2)
N(10)−C(19)	1.15(2)	Rh(2)−Rh(1)−N(8)	88.7(3)
N(2)−C(3)	1.13(2)	Rh(2)−Rh(1)−N(10)	179.0(4)
N(4)−C(7)	1.06(2)	Rh(2)−N(5)−C(9)	160(1)
N(5)−C(9)	1.12(3)	Rh(2)−N(2)−C(3)	177(1)
C(11)−C(12)	1.51(3)	Rh(2)−Rh(1)−N(6)	91.3(4)
	$Rh(MeCN)_6(BF_4)_3$ (**4**)		
Rh(1)−N(1)	1.987(3)	N(1)−Rh(1)−N(4)	91.9(1)
Rh(1)−N(2)	1.984(4)	N(1)−Rh(1)−N(3)	177.9(1)
Rh(1)−N(3)	1.985(3)	Rh(1)−N(2)−C(3)	178.4(4)
Rh(1)−N(4)	1.990(4)		
N(2)−C(3)	1.111(5)		
N(4)−C(7)	1.134(6)		
	$[Rh(CO)_2(MeCN)_2][BF_4]$ (**6**)		
Rh(1)−Rh(1)′	3.1528(14)	C(11)−Rh(1)−N(13)	177.9(3)
Rh(1)−C(11)	1.873(9)	C(11)−Rh(1)−N(14)	92.2(3)
Rh(1)−C(12)	1.858(9)	O(11)−C(11)−Rh(1)	178.3(8)
Rh(1)−N(13)	2.054(7)	C(11)−Rh(1)−Rh(1)′	81.3(3)
Rh(1)−N(14)	2.039(7)		
C(11)−O(11)	1.118(9)		
N(13)−C(13)	1.102(10)		

in the range $20° < 2\theta < 30°$. The crystal was indexed as a centered cell in the monoclinic crystal system, which was verified by axial photography. The intensity of three periodically monitored check reflections decayed by ~40%; thus the program CHORT was applied to compensate for this loss of intensity. The position of the unique Rh atom was determined by the SHELXS-86 program, and the rest of the atoms were located by an alternating series of least-squares refinement and difference Fourier maps. Anisotropic refinement of all nonhydrogen atoms gave residuals of $R = 0.0520$ and $R_w = 0.0807$ with a quality-of-fit index of 2.33. In the last cycle, 235 parameters were refined with 2802 unique data and $F_{obs} > 3\sigma$ of 2395. The shift/esd of the final cycle was 0.13, and the highest remaining peak in the final difference Fourier map was 1.7 $e^-/Å^3$.

b. $[Rh_2^{II,II}(MeCN)_{10}][TFMS]_4$ (2). X-ray quality crystals were grown by layering a solution of **2** with hexanes and diethyl ether in a Schlenk flask that was protected from light for the duration of the diffusion. A crystal of approximate dimensions 0.39 × 0.39 × 0.54 mm^3 was secured with Dow Corning grease on a glass fiber and examined on a Nicolet P3/F diffractometer at 183 ± 2 K. The initial cell determined from 15 film spots was monoclinic primitive, as verified by axial photography. A more accurate cell was obtained by centering on 25 reflections in the range $20° \le 2\theta \le 30°$. The $\theta-2\theta$ scan method was used to collect 7354 final data (6977 unique) between 2θ values of 4°−45°. Check reflections collected every 150 reflections indicated an intensity change of 5%. The structure was solved by the direct methods program, SHELXS-86, which led to the location of the two Rh atoms. The rest of the structure was determined by a series of alternating DIRDIF and difference Fourier maps until the majority of the atoms had been located. Least-squares analyses and Fourier maps were used to complete the structure. After isotropic convergence was achieved, the program DIFABS was applied to correct for absorption. The fluorines of the four CF_3 groups did not refine well as individual atoms; thus each trio of atoms was refined isotropically as a group. All other atoms except the interstitial MeCN solvent molecule were refined anisotropically to give final residuals of $R = 0.075$ and $R_w = 0.091$ with the quality-of-fit indicator equal to 2.35. A final difference map gave the highest remaining peak as 1.5 $e^-/Å^3$ located far from any atoms. All other peaks were less than 1.0 $e^-/Å^3$.

c. $[Rh_2^{II,II}(EtCN)_{10}][BF_4]_4$ (3). Hexagonal rod-shaped crystals of **3** were grown by carefully layering the reaction solution with hexanes followed by diethyl ether. A crystal of dimensions 0.31 × 0.36 × 0.89 mm^3 was mounted on a glass fiber and examined on a Rigaku AFC6S diffractometer. A random search routine located initial reflections to determine a pre-cell from 25 reflections with $20° < 2\theta < 30°$; the symmetry was confirmed as monoclinic C-centered by an automatic Laue check. Data were collected to a maximum 2θ value of 50° at 183 ± 2 K. Three intensity standards collected every 150 reflections displayed no significant decay. The unique Rh atom and immediate coordination sphere were located from the initial direct methods solution, whereas all other nonhydrogen atoms were located and refined from a series of alternating least-squares and difference Fourier maps. The program DIFABS was applied to correct for absorption problems. Two of the ethyl groups were disordered; thus two orientations were each refined at half occupancy. All of the nonhydrogen atoms were refined anisotropically. Final refinement gave residuals of $R = 0.047$ and $R_w = 0.072$ with a goodness-of-fit indicator of 2.27. The last cycle refined with 316 parameters and 3353 data with $F_{obs} > 3\sigma$; the maximum shift/esd was 0.05, and a final difference Fourier showed the highest peak to be 1.04 $e^-/Å^3$ in the map.

d. $[Rh^{III}(MeCN)_6][BF_4]_3$ (4). A yellow crystal of dimensions 0.13 × 0.22 × 0.67 mm^3 was obtained by layering dichloromethane on the reaction solution. The crystal was mounted on a glass fiber using Dow-Corning silicon grease and examined on a Rigaku AFC6S diffractometer. The unit cell was determined by 20 carefully centered reflections in the range $20.96° < 2\theta < 29.14°$. The crystal was determined to be orthorhombic which was verified by axial photography. The structure was solved and refined in the TEXSAN package. The direct methods program SOLVE was used to find the initial Rh atom, after which time DIRDIF was used to locate the rest of the atoms. Full-matrix least-squares refinement of 1621 observed reflections using 168 variable parameters produced residuals of $R = 0.028$ and $R_w = 0.035$ and a

quality-of-fit = 1.39. A final difference map revealed the highest remaining maximum and minimum peaks to be 0.43 and −0.48 $e^-/Å^3$ respectively.

e. $[(Rh(MeCN)_4)(BF_4)_{1.5}]_x$ (5). Brown−red X-ray quality needles of **5** were grown by electrocrystallization as described in the Experimental Section. A specimen of approximate dimensions 0.04 × 0.04 × 0.32 mm^3 was mounted on the end of a fiber with silicone grease and collected at 173 ± 2 K on a Bruker SMART system in the range $4° < 2\theta < 54°$. The crystal system was found to be hexagonal and the space group to be $P6_222$. The data consisted of 11859 measured reflections, 1625 of which were unique, of which 1276 were of the type $F^2_o \geq 4\sigma(F^2_o)$. These 1276 reflections were used to refine 98 parameters to residuals of $R = 0.049$ and $wR2 = 0.0786$ and a goodness of fit =1.19 in the SHELXTL 5.0 software package. Minimum and maximum transmission factors are 0.79 and 0.91, respectively. The highest peak in the final difference map was 0.527 $e^-/Å^{-3}$.

f. $[Rh^I(CO)_2(MeCN)_2][BF_4]$ (6). Bronze needles of $[Rh^I(CO)_2(MeCN)_2][BF_4]$ were prepared by vapor diffusion of diethyl ether into a saturated acetonitrile solution of the compound. A crystal of dimensions 0.14 × 0.23 × 0.34 mm^3 was mounted on a glass fiber, secured with silicone grease, and transferred to the Bruker Smart CCD system. The crystal was cooled to 173 ± 2 K during data collection via a cold stream of nitrogen gas. Examination of the systematic absences and cell symmetry indicated a C-centered monoclinic *C*2/*c* space group, but it did not initially solve in this space group. It was subsequently solved and developed in the P1 group by direct methods and refined in the SHELXTL 5.0 software package. Symmetry operations were then manually added, and the refinement finally converged in *C*2/*c* with a final *R*1 of 0.066 and a *wR*2 of 0.1688 at a resolution of 0.9 Å. The final refinement was based on 146 parameters and 3527 reflections, 1584 of which were unique.

III. Results and Discussion.

A. $[Rh_2(MeCN)_{10}][BF_4]_4$, (1). 1. Synthesis.

$$Rh_2(OAc)_4(MeOH)_2 + 4[Et_3O][BF_4] \xrightarrow[10\ days]{\Delta,\ MeCN} [Rh_2(MeCN)_{10}][BF_4]_4 + 4EtOAc \quad (1)$$

(1)

60−70% yield

$$Rh_2(O_2CCF_3)_4 + 4[Et_3O][BF_4] \xrightarrow[5\ days]{\Delta,\ MeCN} [Rh_2(MeCN)_{10}][BF_4]_4 + 4EtO_2CCF_3 \quad (2)$$

(1)

85% yield

$$Rh_2(OAc)_4(MeOH)_2 + 4HBF_4{\cdot}Et_2O \xrightarrow[7\ days]{\Delta,\ MeCN} [Rh_2(MeCN)_{10}][BF_4]_4 + 4HOAc \quad (3)$$

(1)

60−70% yield

Homoleptic acetonitrile dirhodium cations have been prepared by several different routes. As previously mentioned, one method uses $[EtO_3][BF_4]$ to alkylate the carboxylate ligands in dirhodium tetraacetate (eq 1). This reaction is performed with an excess of the triethyloxonium reagent in order to drive the reaction to completion, since a portion of the reagent is lost to a competing side reaction of $[Et_3O][BF_4]$ with MeCN to yield $[MeCNEt]^+[BF_4]^-$. This method involves a long reaction time (from 10 days to three weeks). Shorter reaction times and lower temperatures yield product admixed with the persistent intermediate *cis*-$[Rh_2(OAc)_2(MeCN)_6]^{2+}$ which is much less soluble than $[Rh_2(MeCN)_{10}][BF_4]_4$ in the CH_3CN/CH_2Cl_2 mixtures. The crude product may appear red by casual examination, but careful scrutiny reveals the presence of both purple and orange crystals. The mixtures are easily identified by ^1H NMR spectroscopy; resonances are present at $\delta = 2.31$ and $\delta = 2.03$ for $[Rh_2(OAc)_2(MeCN)_6]^{2+}$ in addition to singlets at $\delta = 2.74$ and $\delta = 2.45$ for $[Rh_2(MeCN)_{10}][BF_4]_4$. The impurity can also be detected in the IR spectrum, with four ν(C≡N) stretches appearing between 2340 and 2249 cm^{-1} for a mixture of both compounds, as compared to only three features, namely, 2345, 2317, and 2287 cm^{-1} for pure $[Rh_2(MeCN)_{10}][BF_4]_4$. No evidence of tris-acetate or mono-acetate intermediates was detected, which suggests that the bridging ligands are removed in pairs.

In an effort to decrease the time required to synthesize $[Rh_2(MeCN)_{10}][BF_4]_4$, the more labile starting material $Rh_2(O_2CCF_3)_4$ was used (eq 2), and, indeed, reaction times with this precursor are typically one week or less as compared to 10 days to three weeks beginning with $Rh_2(OAc)_4(MeOH)_2$.

A third strategy for the synthesis of $[Rh_2(MeCN)_{10}][BF_4]_4$ is the treatment of $Rh_2(OAc)_4(MeOH)_2$ with $HBF_4{\cdot}Et_2O$. The acid is used to protonate the bridging carboxylate ligands, thereby liberating acetic acid. The reaction with $HBF_4{\cdot}Et_2O$ is rather slow (eq 3) as is the case with the $[Et_3O][BF_4]$ reagent, with yields of the product after crystallization being the same or slightly lower than those from the alkylation reaction. A disadvantage of the acid method is that it leads to more severe oiling problems; thus it is necessary to perform several recrystallizations before a pure sample of $[Rh_2(MeCN)_{10}][BF_4]_4$ can be obtained.

2. Spectroscopic Properties. $[Rh_2(MeCN)_{10}][BF_4]_4$ displays a broad, intense IR feature at 1065 cm^{-1} due to the $[BF_4]^-$ stretches and three resonances at 2345, 2315, and 2287 cm^{-1} attributable to ν(C≡N) stretches. Solution infrared spectra in CH_3NO_2 revealed that the modes due to the equatorial ligands are not affected (2342 (vs), 2314 cm^{-1}(s)) but that free CH_3CN is present at 2254 cm^{-1} due to axial ligand exchange with nitromethane. A ^1H NMR spectrum of **1** in CD_3NO_2 displays two resonances, one singlet at $\delta = 2.74$ due to equatorial MeCN and a broad feature at $\delta = 2.42$ attributed to the exchanged axial groups. This spectrum is invariant over the course of 7 days. The breadth of the resonance at $\delta = 2.42$ indicates that rapid exchange is occurring at the axial sites.[22] The lability of the axial positions is so high, in fact, that axial exchange reactions of $[Rh_2(MeCN)_{10}]^{4+}$ occur even in the solid state, as evidenced by the color changes of suspensions of $[Rh_2(MeCN)_{10}][BF_4]_4$ in MeOH (red), THF (pale orange), or acetone (olive green). Isolation of the solids and investigation by infrared spectroscopy show a disappearance of the lowest-energy ν(C≡N) mode at 2287 cm^{-1}, which is assigned to the axial MeCN. The equatorial modes experience slight shifts (CaF_2, cm^{-1}): MeOH, 2341 (s), 2317 (s); THF, 2345 (s), 2316 (s); acetone, 2332 (w), 2311 (w).

Electronic spectra of anaerobic solutions of $[Rh_2(MeCN)_{10}]^{4+}$ prepared in the dark display two absorptions at λ_{max} values of 468 and 270 nm. Aerobic sample preparation in the presence of light leads to an additional feature at 365 nm, which is caused by the photochemical sensitivity of the compound. An analysis of the photochemical behavior of this compound has been published, and the reader is directed to ref 14 for additional details on this topic.[14]

3. Crystal Structure. An ORTEP diagram of $[Rh_2(MeCN)_{10}][BF_4]_4$, depicted in Figure 1, clearly shows that the dirhodium cation is in an octahedral environment. The center of the Rh−Rh bond resides on a crystallographic C_2 axis, and the equatorial planes of MeCN ligands are twisted with respect to each other ($\chi_{av} = 44.8(2)°$). The axial MeCN groups deviate somewhat

(22) Pittet, P.-A.; Dadci, L.; Zbinden, P.; Abouhamdan, A.; Merbach, A. E. *Inorg. Chim. Acta* **1993**, *206*, 135.

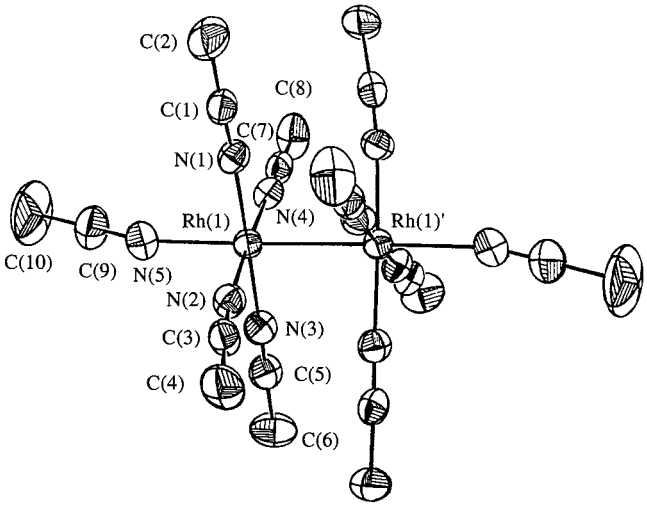

Figure 1. ORTEP drawing of the cation in **1**, $[Rh_2(MeCN)_{10}][BF_4]_4$, with 50% probability ellipsoids.

from linearity which reduces the molecular symmetry from idealized D_{4d} symmetry to C_2. While this is not the first example of an unbridged Rh−Rh bond, it represents a rare example of this unit in the absence of any significant repulsion between ligands.[23] The longest distance for a Rh(II)−Rh(II) bond to date is 2.936 Å found in the $Rh_2(dmg)_4(PPh_3)_2$ molecule, in which the equatorial ligands are close to achieving the maximum torsion angle.[24] The added presence of bulky axial PPh_3 groups prevents the ligands from further relieving steric repulsion by bending away from each other, and as a result, the metal−metal distance lengthens. The Rh−Rh bond distance in **1** of 2.624(1) Å is much shorter than the other unbridged examples, but is still longer than the average length of 2.35−2.45 Å in tetra-bridged systems.[25] It must be noted that the bridged systems generally employ anionic π-donor ligands as opposed to neutral σ-donors such as those used in the present study; therefore comparisons are necessarily limited.

B. Salts of $[Rh_2^{II,II}(RCN)_{10}]^{4+}$ with Increased Solubility. 1. $[Rh_2^{II,II}(MeCN)_{10}][TFMS]_4$, (2). a. Synthesis and Spectroscopic Properties. Tetrafluoroborate salts display limited solubilities in common solvents; consequently substitution reactions of $[Rh_2(MeCN)_{10}][BF_4]_4$ must be performed in polar, coordinating solvents such as MeCN, H_2O, CH_3NO_2, and DMSO. In principle, anion exchange via simple metathesis is the most straightforward way of preparing new salts, but efforts to this end with *p*-toluenesulfonate or triflate salts led only to inseparable mixtures. Reactions of $Rh_2(OAc)_4$ with reagents such as methyl triflate or triflic acid yielded intractable red−orange oils. The use of the unusual reagent $Me_3Si(TFMS)$ to convert acetate ligands on $Rh_2(OAc)_4(MeOH)_2$ to silylesters as shown in eq 4 ultimately led to the successful isolation of crystalline $[Rh_2(MeCN)_{10}][TFMS]_4$.

$$Rh_2(OAc)_4(MeCN)_2 + 4Me_3Si(TFMS) \xrightarrow[7\ \text{days}]{\Delta,\ MeCN} [Rh_2(MeCN)_{10}][TFMS]_4 + 4Me_3SiOAc \quad (4)$$

(**2**)
73% yield

Trimethylsilyl reagents have proven to be very effective at removing carboxylate ligands from dinuclear units, but typically the reagent is of the type Me_3SiX (X = Cl, Br, or I).[26] In these reactions, the halide replaces the liberated anionic carboxylate to maintain the original charge on the compound. In the present case, the noncoordinating anion $[TFMS]^-$ is present, which allows the solvent to replace the esterified carboxylate.

A major difference in the solid-state properties of the $[BF_4]^-$ and $[TFMS]^-$ salts was observed; specifically when the $[TFMS]^-$ salt is subjected to a dynamic vacuum for several hours, the orange microcrystalline compound converts to a purple powder. ^1H NMR spectra recorded in CD_3NO_2 revealed that the purple compound displays a single resonance at $\delta = 2.79$, while the spectrum of the orange compound under the same conditions shows a resonance for the equatorial ligands at $\delta = 2.79$ as well as an axial feature at $\delta = 2.02$. Solution IR spectra in CH_3NO_2 of the purple compound exhibit two stretches in the ν(C≡N) region at 2340 and 2311 cm^{-1}, and the orange solid exhibits these two modes as well as a feature due to free MeCN at 2253 cm^{-1}. $[Rh_2(MeCN)_{10}][TFMS]_4$ displays three ν(C≡N) stretches at 2345, 2316, and 2286 cm^{-1} in the solid state, while the spectrum of the purple compound is missing the lowest-energy stretch due to the axial ligands.

The solid-state behavior of $[Rh_2(MeCN)_{10}][TFMS]_4$ is in accord with the loss of the weakly held axial MeCN ligands from the $[Rh_2(MeCN)_{10}]^{4+}$ cation which causes a change in the chromophore responsible for the color of the compound, namely, the π^*-σ^* transition.[25] Two different scenarios can be envisioned in this case; the axial position may be vacant, as in the case of $Rh_2(O_2CCF_3)_4$, or it may be occupied by the triflate anion.

$[Rh_2(MeCN)_{10}][TFMS]_4$ dissolves in acetone and alcohols with pronounced color changes indicative of solvent exchange. A ^1H NMR spectrum in d^6-acetone supports the conclusion of long-term instability in this solvent. If the sample is measured immediately after dissolution, there is a single resonance at $\delta = 2.91$, but within 24 h the red solution becomes olive green with multiple resonances appearing at $\delta = 2.95$, 2.91, 2.85, and 2.76. The complexity of the spectrum indicates that the material is a mixture of species. In a similar vein, prolonged exposure to MeOH at high concentrations results in the precipitation of a black solid from an olive-green solution.

b. Crystal Structure. The different counterions in **1** and **2** are sufficient to cause a symmetry change from a C-centered (**1**) to a primitive monoclinic (**2**) crystal system. An ORTEP diagram of the cation is depicted in Figure 2. The packing diagrams of the cations, shown in Figure 3a,b, reveal that the $[TFMS]^-$ salt is more loosely packed than the $[BF_4]^-$ salt. Indeed the unit cell of the triflate salt contains enough void space to incorporate an interstitial acetonitrile molecule, unlike the more densely packed $[BF_4]^-$ structure. Although the packing is quite different in the two salts, the molecular structures of the cations in **1** and **2** are virtually identical. The Rh−Rh bond distance of 2.617(2) Å in **2** is comparable to the value of 2.624(1) Å in **1**. The torsion angle is slightly less than perfectly staggered at 42.8(5)°, but otherwise, crystal-packing forces do not appear to substantially influence either the conformation or the local environment of the dirhodium cation.

2. $[Rh_2(EtCN)_{10}][BF_4]_4$, (3). a. Synthesis. Another strategy for increasing the solubility of the solvated dirhodium species in less polar solvents is to add a longer alkyl chain substituent

(23) Cotton, F. A.; Walton, R. A. *Multiple Bonds Between Metal Atoms*, 2nd ed.; Clarendon Press: Oxford, U.K., 1993.
(24) Caulton, K. G.; Cotton, F. A. *J. Am. Chem. Soc.* **1969**, *91*, 6517. Caulton, K. G.; Cotton, F. A. *J. Am. Chem. Soc.* **1971**, *93*, 1914.
(25) Felthouse, T. R. *Prog. Inorg. Chem.* **1982**, *29*, 73.
(26) See for example: (a) Cotton, F. A.; Dunbar, K. R. *J. Am. Chem. Soc*. **1987**, *109*, 3142. (b) Cotton, F. A.; Dunbar, K. R.; Verbruggen, M. G. *J. Am. Chem. Soc*. **1987**, *109*, 5498. (c) Cotton, F. A.; Dunbar, K. R.; Matusz, M. *Inorg. Chem*. **1986**, *25*, 3641. (d) Cotton, F. A.; Dunbar, K. R.; Poli, R. *Inorg. Chem*. **1986**, *25*, 3700. (e) Campbell, F. L.; Cotton, F. A.; Powell, G. L. *Inorg. Chem*. **1984**, *23*, 4222.

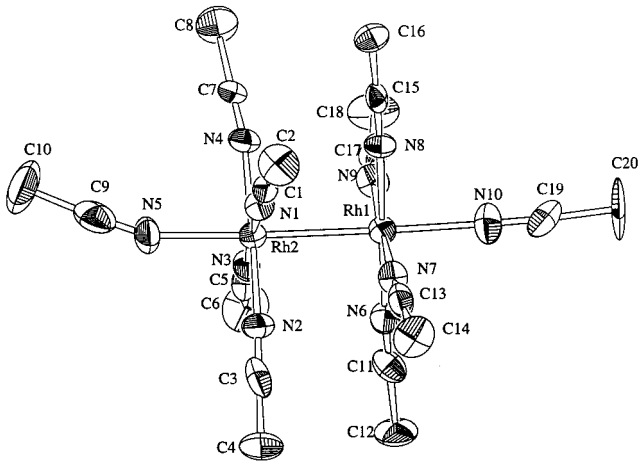

Figure 2. ORTEP drawing of the cation in **2**, $[Rh_2(MeCN)_{10}][TFMS]_4$, with 50% probability ellipsoids.

to the nitrile. A space-filling model of $[Rh_2(MeCN)_{10}][BF_4]_4$ reveals no significant steric repulsions between the staggered ligands; therefore we reasoned that it would be possible to replace MeCN with other RCN groups without disrupting the dimetal unit. Attempts to synthesize $[Rh_2(EtCN)_{10}][BF_4]_4$ by solvent exchange of propionitrile for acetonitrile did not proceed cleanly, however, as judged IR and NMR spectroscopy. A better approach for the synthesis of the desired compound proved to be directly from $Rh_2(OAc)_4(MeCN)_2$ and HBF_4 in propionitrile as depicted in eq 5. The loss of carboxylate ligands proceeds

$$Rh_2(OAc)_4(MeCN)_2 + 4HBF_4{\cdot}Et_2O \xrightarrow[2\ \text{days}]{\Delta,\ EtCN} [Rh_2(EtCN)_{10}][BF_4]_4 + 4HOAc \quad (5)$$

(**3**)
67% yield

much faster in propionitrile than in acetonitrile, but workup involves several iterations of recrystallization due to a tendency of the solutions to oil. Attempted preparations of the triflate salt of the propionitrile complex using reagents such as HTFMS or $Me_3Si(TFMS)$ with $Rh_2(OAc)_4(MeCN)_2$ did not yield tractable products. The triflic acid reaction gave a red−orange colored solution, but the reaction with trimethylsilyltriflate produced a brown solution. The greater hygroscopic nature of triflic acid along with the increasing solubility of triflate salts generally complicates the isolation of triflate-based products.

b. Spectroscopic and Physical Properties. The solution behavior of $[Rh_2(EtCN)_{10}][BF_4]_4$ is similar to that of the MeCN compound. Immediately after dissolution in CD_3CN, the expected 4:1 ratio of equatorial to axial EtCN ligands is observed, with full exchange of all sites occurring within 24 h. An FT-IR spectrum displays only two stretches in the ν(C≡N) region at 2324 and 2287 cm^{-1}. A broad ν(B−F) stretch appears at 1055 cm^{-1}.

c. Crystal Structure. The thermal ellipsoid plot for the cation $[Rh_2(EtCN)_{10}]^{4+}$ is shown in Figure 4 with only one orientation of the disordered ligands presented for clarity. Despite the additional CH_2 group on the nitrile ligands in $[Rh_2(EtCN)_{10}]^{4+}$, the salt packs in the same manner as the MeCN derivative, as illustrated in Figure 3a,c. The center of the Rh−Rh bond lies on a 2-fold axis, rendering one-half of the molecule and two of the $[BF_4]^-$ ions unique. The torsion angle is essentially ideal at 44.9(2)°. Two equatorial ethyl groups are disordered in two orientations, namely, C5/C6 and C11/C12. It is somewhat surprising that only two of the five groups displayed any

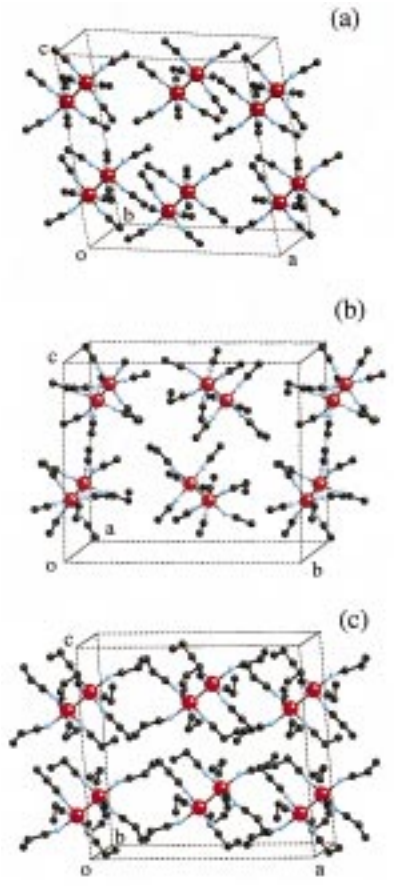

Figure 3. Packing diagrams of the dirhodium cations in (a) **1** in the xz plane (b) **2** in the yz plane and (c) **3** in the xz plane.

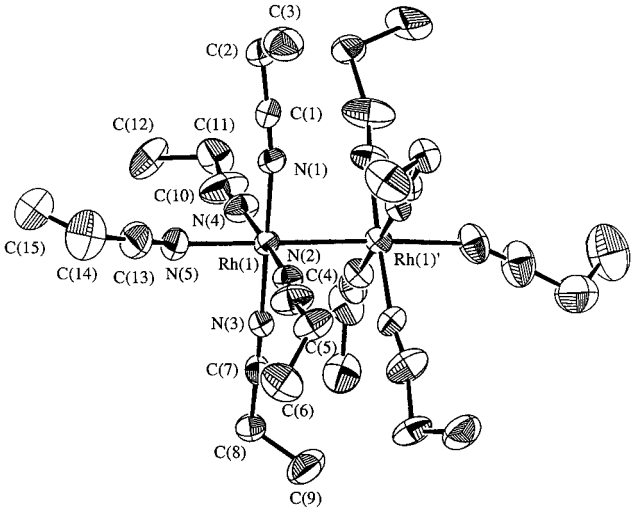

Figure 4. ORTEP diagram of **3**, $[Rh_2(EtCN)_{10}][BF_4]_4$, with 50% thermal ellipsoids. Only one orientation of the two disordered ethyl groups is shown.

significant disorder, even though multiple orientations become more likely with the increasing length of the alkyl group. The Rh−Rh bond distance of 2.6040(9) Å falls in the same range as the other two nitrile salts, which suggests that the Rh−Rh bond is not highly influenced by the identity of the ligand or different counterions.

C. Redox Chemistry of $[Rh_2(MeCN)_{10}][BF_4]_4$. 1. Electrochemistry. A cyclic voltammogram of $[Rh_2(MeCN)_{10}][BF_4]_4$ performed in 0.1 M $TBABF_4$ in MeCN displays a single

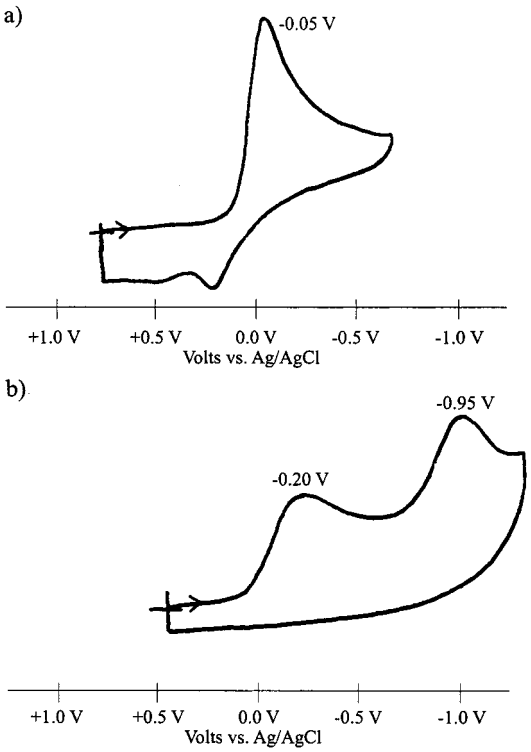

Figure 5. Cyclic voltammograms for (a) $[Rh_2(MeCN)_{10}][BF_4]_4$ in MeCN and (b) $[Rh_2(EtCN)_{10}][BF_4]_4$ in EtCN (0.2 M $[Bu_4N][BF_4]$, Pt working electrode, Ag/AgCl reference).

irreversible reduction at $E_{p,c} = -0.05$ V vs Ag/AgCl (-0.54 V vs Fc/Fc^+) as shown in Figure 5a. This reduction corresponds to the formation of **5** as explained in a later section.[14] The absence of an accessible oxidation (typically exhibited by Rh_2-(II,II) compounds)[25] is not surprising due to the high positive charge localized on the metal centers. $[Rh_2(EtCN)_{10}][BF_4]_4$ (Figure 5b) displays an irreversible reduction at $E_{p,\,c} = -0.20$ V vs Ag/AgCl (-0.625 V vs Fc/Fc^+), located at a slightly more negative potential than $[Rh_2(MeCN)_{10}][BF_4]_4$, and a second irreversible reduction $E_{p,c} = -0.95$ V vs Ag/AgCl (-1.375 vs Fc/Fc^+).

2. Chemical Oxidation to $[Rh(MeCN)_6][BF_4]_3$. Despite the c.v. data, which showed an absence of accessible oxidation processes for $[Rh_2(MeCN)_{10}]^{4+}$, the mononuclear homoleptic cation $[Rh^{III}(MeCN)_6][BF_4]_3$ does, in fact, exist. It was first detected as a contaminant in batches of $[Rh_2^{II,II}(MeCN)_{10}][BF_4]_4$ prepared from $Rh_2(OAc)_4$ and $[Et_3O][BF_4]$. Since electrochemical oxidation in acetonitrile is not accessible as judged by the cyclic voltammogram, we turned to the use of chemical oxidants. It was found that $[Rh_2^{II,II}(MeCN)_{10}][BF_4]_4$ reacts with $NOBF_4$ to form the Rh^{III} salt, as indicated in eq 6.

$$[Rh_2^{II}(MeCN)_{10}][BF_4]_4 + 2NOBF_4 \xrightarrow[4\ \text{hours}]{\Delta,\ MeCN} [Rh^{III}(MeCN)_6][BF_4]_3 + 2NO_{(g)} \quad (6)$$

(4)
33% yield

As for a possible mechanism of the reaction, it is logical to propose that NO^+ binds to a labile axial site on the dinuclear complex to form an unstable intermediate that undergoes inner-sphere electron transfer between the Rh^{II} center and NO^+. Expulsion of the reduction product, NO, would be expected, as π-acceptor ligands are known to be incompatible with the Rh^{III} oxidation state. Metal−metal bond cleavage is also anticipated due to the high stability of low-spin d^6 octahedral complexes.[27] This route is obviously not a clean oxidation of the $Rh_2^{II,II}$ dinuclear compound to the mononuclear Rh^{III} homoleptic acetonitrile species, however, as evidenced by the low yields (~35%) and the persistence of an oily green byproduct.

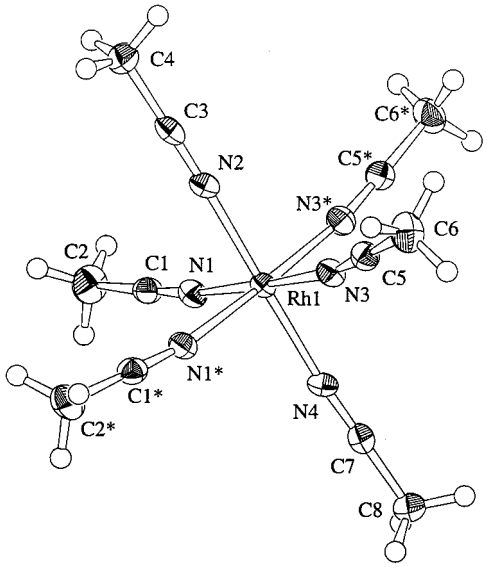

Figure 6. An ORTEP diagram of $[Rh(MeCN)_6][BF_4]_3$, **4**, with 50% thermal ellipsoid plot.

An IR spectrum of $[Rh(MeCN)_6][BF_4]_3$ displays a single $\nu(C{\equiv}N)$ stretch at 2358 cm^{-1}, which is at higher energies than the modes in the parent compound (2342, 2317, and 2287 cm^{-1}). A ^1H NMR spectrum of this compound displays a singlet at $\delta = 2.76$ with no evidence for exchange on the NMR time scale, which is not unexpected for a substitutionally inert d^6 low-spin Rh^{III} complex.[26]

The molecular structure of $[Rh^{III}(MeCN)_6][BF_4]_3$ is octahedral with an average Rh−N distance of 1.987 Å (Figure 6), which is slightly shorter than analogous distances found in other nitrogen-bound homoleptic Rh^{III} complexes. For example, $[Rh(en)_3]^{3+}$ and $[Rh(2,2'\text{-bpy})_3]^{3+}$ exhibit average Rh−N distances of 2.077 and 2.015 Å, respectively.[28a−d] As far as we are aware, there are no other crystallographically determined Rh^{III} compounds in the literature that contain six monodentate nitrogen donor ligands; all documented examples involve bidentate ligands.

3. Reduction to $[Rh^{I,II}(MeCN)_4(BF_4)_{1.5}]_x$ (5). a. Synthesis and Physical Characterization. A cyclic voltammogram of $[Rh_2(MeCN)_{10}][BF_4]_4$ recorded in MeCN displays an irreversible reduction at -0.05 V vs Ag/AgCl in MeCN. Although a variety of reagents can be used to chemically achieve this reduction ($CoCp_2$, Zn etc.), it was not possible to isolate a pure form of the compound by these methods. Electrochemical reduction of $[Rh_2^{II,II}(MeCN)_{10}][BF_4]_4$ at a Pt electrode in a two-compartment cell by a controlled current method provides a more convenient approach to the production of a crystalline material.[13,14] A one-electron reduction of the singly bonded $Rh_2^{II,II}$ cation involves a population of the σ^* orbital to give what is obviously an unstable $Rh_2^{I,II}$ radical. As with the case of many organic radicals, the metallo-radical "monomer" unit oligomerizes, with

(27) Cotton, F. A.; Wilkinson, G. *Advanced Inorganic Chemistry*, 5th ed.; Wiley: New York, 1988.

(28) (a) Gargallo, M. F.; Tapscott, R. E.; Duesler, E. N. *Inorg. Chem.* **1984**, *23*, 918. (b) Hoffmann, S. K.; Hodgson, D. J.; Hatfield, W. E. *Inorg. Chem.* **1985**, *24*, 1194. (c) Traylor, T. G.; Tsuchiya, S. *Inorg. Chem.* **1987**, *26*, 1338. (d) Miyamae, S. O.; Sato, S.; Saito, Y. *Acta Crystallogr., Sect. B* **1979**, *35*, 1470.

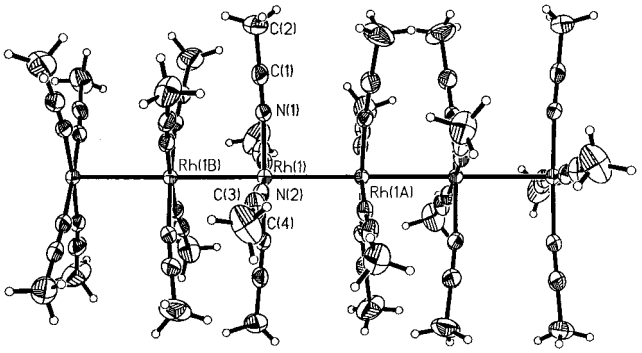

Figure 7. An ORTEP diagram of $[Rh(MeCN)_4(BF_4)_{1.5}]_x$, **5**, with a 50% thermal ellipsoid plot.

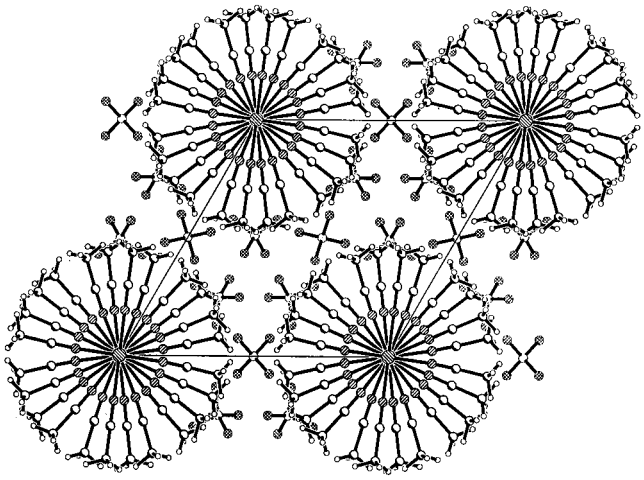

Figure 8. View of the unit cell packing of **5** along the c direction.

the final result being an insoluble polymeric product of general formula $[Rh(MeCN)_4(BF_4)_{1.5}]_x$.

The extended rhodium chain material $[Rh(MeCN)_4(BF_4)_{1.5}]_x$ displays two extremely weak $\nu(C{\equiv}N)$ modes in the IR spectrum at 2328 and 2299 cm^{-1}. These are significantly lower in energy than the stretches located at 2345 and 2315 cm^{-1} in $[Rh_2(MeCN)_{10}][BF_4]_4$. Considering the lower-valence state of the rhodium ions in the mixed-valence chain, one may expect less σ-donation and increased π-back bonding for the MeCN ligands, which would lead to a slight decrease of the $\nu(C{\equiv}N)$ bond order.

b. Crystal Structure. Views of the cation chains in $[Rh(MeCN)_4(BF_4)_{1.5}]_x$ are depicted in Figures 7 and 8. As implied by the formula, $[Rh(MeCN)_4(BF_4)_{1.5}]_x$ is composed of a polymeric chain of rhodium ions in a square planar environment of MeCN ligands. There are only several examples in the literature in which $Rh^{I,II}$ mixed-valence systems are found to be oligomeric, and there are no previous examples of a 1-D chain structure for such species.[29a−c] The compound crystallizes in the $P6_222$ space group with the cations residing on a 6_2 screw axis, which does not require adjacent Rh−Rh bond distances to be identical. Indeed, two different contacts, a short (2.8442(8) Å) and a long (2.9277(8) Å) one, are present in the chain. Both distances are significantly longer than the Rh−Rh single bond of 2.624(1) Å in $[Rh_2(MeCN)_{10}][BF_4]_4$, but they are considerably shorter than typical Rh^I−Rh^I contacts as exemplified by **6**, which contains Rh^I−Rh^I interactions of ∼3.16 Å. As the diagrams indicate, two different sets of torsion angles for the equatorial

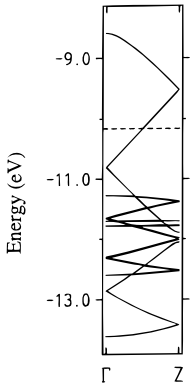

Figure 9. Calculated dispersion relations for the d-block bands of the $[Rh(MeCN)_4]^{1.5+}$ chain. The dotted line refers to the hypothetical Fermi level assuming double occupancy of the levels.

MeCN ligands are present, namely, 44.8° between the Rh atoms with the shorter contacts and 15.3° between the Rh atoms at the longer separations. It is noted that there is a slight "bending" of the acetonitrile ligands away from each other in the "dimer" with the smaller torsion angle, which suggests that a slight steric effect is operative at a $\chi = 15.3°$, which is alleviated when $\chi = 44.8°$.

c. Physical Properties. The calculated band structure for a $[\{Rh(MeCN)_4\}_6]^{9+}$ chain is shown in Figure 9. Since the unit cell of the chain contains six $Rh(MeCN)_4$ units, the bands in Figure 9 appear as six, folded bands; that is, every band appears as containing six subbands. Essentially, the band structure contains a dispersive z^2 band, which in the lower part of the diagram overlaps with a series of flatter bands originating from the xy, xz, and yz orbitals of the square planar monomer. Because of the dimerization, there is a gap between the third and fourth z^2 subbands (i.e., at the middle of the z^2 band), but there is no gap between the other subbands. As a result of the stoichiometry the second subband from the top would be half filled if there was double occupancy of the levels (i.e., assuming a metallic-type filling). Consequently, if the metallic state of this material could be realized, the material is expected to undergo a metal to insulator Peierls-type distortion, which would double the size of the unit cell.

Alternatively, the presence of the dimeric units in the chain suggests a possible localized description of the electronic structure of **5**. The chain can be viewed as a series of $[Rh(MeCN)_4]_2^{3+}$ dimers with two electrons in the bonding combination (Ψ^+) of the two z^2 orbitals of one dimer and one electron in the antibonding combination (Ψ^-). Thus, in this description, every dimer will carry one unpaired electron. It should be noted that the total width of the z^2 band in Figure 9 is quite large. In fact the dispersion of the upper group of three subbands, which are essentially built from the Ψ^- orbital, is as large as the z^2 band of KCP calculated with the same method.[30] Obviously a band description is not appropriate for a localized system, but these results suggest that the Ψ^- levels interact appreciably along the chain; that is, the transfer integral between two adjacent Ψ^- orbitals is quite strong. In other words, if the localized description is applicable, the successive unpaired electrons interact quite strongly. In view of these data, we believe that it is not unreasonable to predict that a metallic state for the chain could be stabilized under pressure.

The temperature dependence of the electrical conductivity of the mixed-valence chain compound, **5**, was measured on a single crystal at ambient pressure in the temperature range of

(29) (a) Chern, S.-S.; Lee, G.-H.; Peng, S.-M. *J. Chem. Soc., Chem. Commun.* **1994**, 1645. (b) Mann, K. R.; DiPierro, M. J.; Gill, T. P. *J. Am. Chem. Soc.* **1980**, *102*, 3965. (c) Sigal, I. S.; Mann, K. R.; Gray, H. B. *J. Am. Chem. Soc.* **1980**, *102*, 7252.

(30) Whangbo, M.-H.; Hoffmann, R. *J. Am. Chem. Soc.* **1978**, *100*, 6093.

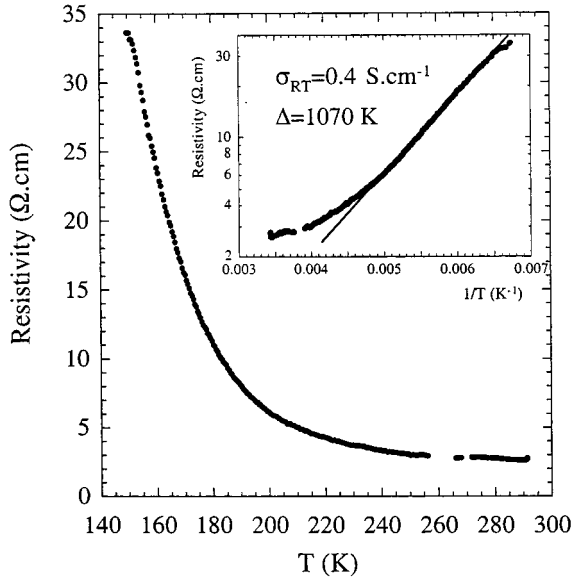

Figure 10. Temperature dependence of the resistivity for **5**.

150−300 K. A plot of the resistivity, R (Ω cm), vs T is shown in Figure 10. With decreasing temperature, the resistivity increases exponentially ($R = R_{rt} + a \exp(E/T)$) between room temperature and 150 K, which is typical for a semiconductor. The conductivity at rt is approximately $\sigma = 0.5-2$ S cm^{-1}, and the activation energy $E_a \sim 500$ K.[31] These values suggest a localization of the charge carriers, as frequently found in 1-D compounds.[32]

Figure 11 depicts the evolution of the EPR line as a function of temperature. One broad line is observed at room temperature (Figure 11a) with a g value of 2.1679 and a line width of $\Delta H = 234$ G. With decreasing temperature (Figure 11b,c), the line width becomes much more narrow and two g values at 2.1991 and 1.9972 (at 80 K) appear in accord with axial Rh^{II} systems.[33] The less intense, sharper features (ΔH in the range 10−30 G) between the two g values are due to the polycrystalline nature of the sample, and indeed, rotation of the sample in the cavity from 0° to 90° (Figure 11b,c) clearly reveals an influence of the orientation of the few crystals on the signal. At 4.2 K (Figure 11d), the position of the g value does not change but the line width increases and the intensity of the signal decreases dramatically (Figure 12).

The variable temperature magnetic susceptibility properties of a powder sample of $[Rh(MeCN)_4(BF_4)_{1.5}]_x$ were measured with the use of a SQUID magnetometer. Temperature-independent paramagnetism (1×10^{-4} emu CGS/mol) was observed down to 40 K, and a Curie paramagnetic impurity was evident

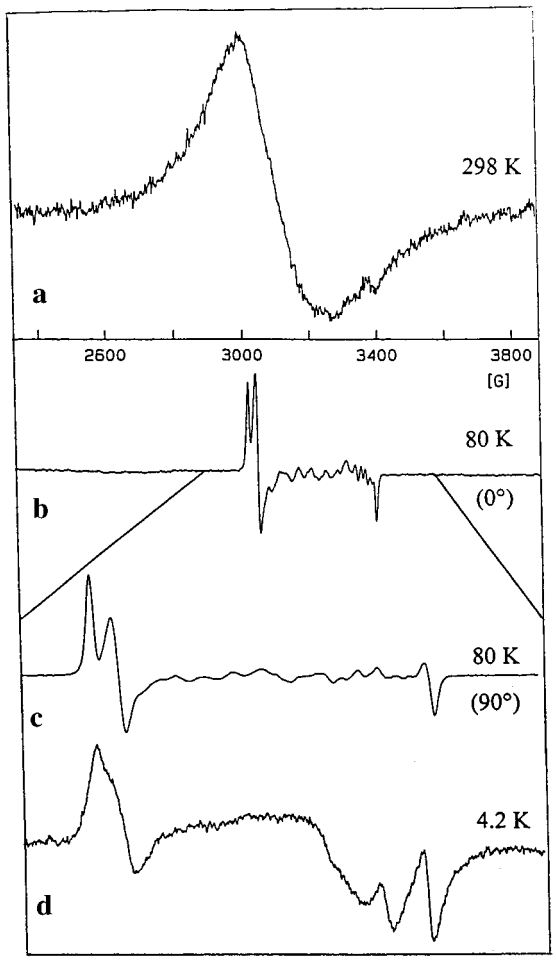

Figure 11. EPR spectra obtained on a few crystals of **5** at (a) 298 K, (b) 80 K, (c) 80 K and rotated 90°, and (d) 4.8 K.

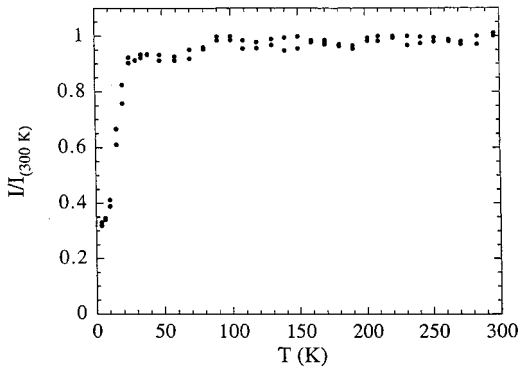

Figure 12. Thermal dependence of the integrated intensity of the resonance EPR lines (normalized at 300 K) obtained on a sample consisting of several single crystals of **5**.

at lower temperatures. This apparent Pauli paramagnetic behavior was confirmed by an integration of the EPR line on a sample consisting of several single crystals (Figure 12); this thermal dependence is typically observed in the case of conductors. Electronic correlations and the 1-D nature of $[Rh(MeCN)_4(BF_4)_{1.5}]_x$ could result in a decoupling of the spin and the charge degrees of freedom. Simply put, localization of the charge (activated law of the resistivity) and the Pauli behavior of the susceptibility are not necessarily incompatible. Indeed, such behavior has been observed in salts such as $(TMTTF)_2PF_6$ (TMTTF = tetramethyltetrathiafulvalene).[34] At low temperatures ($T \sim 20$ K), the magnetic susceptibility decreases abruptly, an

(31) The electrical contacts made with Ag or graphite paste were highly resistive, possibly due to the reactivity of the sample with these materials which may have altered the four probe measurement.

(32) (a) Bray, J. W.; Hart, H. R.; Interrante, L. V.; Jacobs, I. S.; Kasper, J. S.; Waltkins, G. D.; Wei, S. H.; Bonner, J. C. *Phys. Rev. Lett.* **1975**, *35*, 744. (b) Jacobs, I. S.; Bray, J. W.; Hart, H. R.; Interrante, L. V.; Kasper, J. S.; Waltkins, G. D.; Prober, D. E.; Bonner, J. C. *Phys. Rev. B: Solid State* **1976**, *14*, 3036. (c) Huizinga, S.; Kommandeur, J.; Sawatzky, G. A.; Thole, L. V.; Kopinga, K.; de Jonge, W. J. M.; Roos, J. *Phys. Rev. B: Solid State* **1979**, *19*, 4723. (d) Jacobsen, C. S.; Pedersen, H. J.; Mortensen, K.; Bechgaard, K. *J. Phys. C.: Solid State Phys.* **1980**, *12*, 3411. (e) Hase, M.; Terasaki, I.; Uchinokura, K. *Phys. Rev. Lett.* **1993**, *70*, 3651.

(33) (a) Woods, C.; Tortorelli, L. J.; Rillema, D. P.; Burn, J. L. E.; DePriest, J. C. *Inorg. Chem.* **1989**, *28*, 1673. (b) Bear, J. L.; Yao, C. L.; Capdevielle, F. J.; Kadish, K. M. *Inorg. Chem.* **1988**, *27*, 3782. (c) Bunn, A. G.; Wayland, B. B. *J. Am. Chem. Soc.* **1992**, *114*, 6917. (d) Dunbar, K. R.; Haefner, S. C.; Pence, L. E. *J. Am. Chem. Soc.* **1989**, *111*, 5504. (e) Dunbar, K. R.; Haefner, S. C. *J. Am. Chem. Soc.* **1991**, *113*, 9540. (f) Dunbar, K. R.; Haefner, S. C. *Organometallics* **1992**, *11*, 1431.

instability that has also been noted for the $(TMTTF)_2PF_6$ and other 1-D materials.[32] This may be a signature of a Spin-Peierls transition in this system, which, in localized spin systems, is analogous to the Peierls transition in conductors. Such behavior is not surprising in view of the aforementioned relatively strong interaction between the Ψ^- orbitals of two adjacent dimers of the chain, which are the spin carriers. These "Rh dimers" can be considered to be part of a regular chain of $S = {}^1/_2$ spin centers. At $T > 20$ K, the energies of the magnetic orbitals are degenerate, and all of the exchange constants between dimers are identical; the spins remain unpaired but are antiferromagnetically coupled. At $T < 20$ K and below, the behavior is consistent with a structural distortion that serves to remove the degeneracy by introducing two exchange constants. In this configuration, the spins populate the lower orbital energy and form a pair; consequently the ground state is no longer magnetic.

The conductivity and magnetic behavior of the unprecedented metal−metal bonded chain $[Rh(MeCN)_4(BF_4)_{1.5}]_x$ reveal interesting behavior, analogous to that of materials such as $[TMTTF]_2[PF_6]$. The Spin-Peierls transition is one of the most interesting phenomena manifested by low-dimensional quantum-spin systems; thus detailed conductivity measurements (including those under pressure) and additional magnetic measurements are in progress to confirm this transition and to fully elucidate the nature of the low temperature state.

D. $[Rh^I(CO)_2(MeCN)_2]^+$, (6). 1. Synthesis. The salt $[Rh(CO)_2(MeCN)_2][BF_4]$, originally isolated from CO trapping of a Rh^{III} intermediate generated by photochemical irradiation of $[Rh_2(MeCN)_{10}][BF_4]_4$, has been explored as a possible precursor for the unknown monovalent acetonitrile cation $[Rh^I(MeCN)_4]^+$. A rational, high-yield synthesis of $[Rh(CO)_2(MeCN)_2][BF_4]$ is conveniently performed by abstraction of chloride ions from $Rh_2(\mu\text{-}Cl)_2(CO)_2$ by $AgBF_4$ in acetonitrile.[35] Upon treatment with diethyl ether or evaporation of the solvent, the yellow solution of (**6**) produces a dark blue solid. This behavior hints at the presence of Rh^I-Rh^I contacts in the solid state brought about by stacking of the square planar molecules.[36]

2. Spectroscopic Properties. ^1H NMR and IR spectroscopic properties of the cation $[Rh(CO)_2(MeCN)_2]^+$ have been described elsewhere; thus no details of these will be provided.[13,37] One issue, however, that has not been addressed in prior studies is the loss of one of the CO ligands under reduced pressure. The acetonitrile solution IR spectrum of $[Rh(CO)_2(MeCN)_2]^+$ in a CaF_2 cell contains two ν(CO) modes at 2121 and 2064 cm^{-1} in accord with a cis geometry. When the solution of the compound is placed under reduced pressure, however, the two IR features begin to disappear, and a new absorption appears at 2037 cm^{-1}, consistent with the formation of a monocarbonyl species. Introduction of CO gas into the solution reverses this reaction and converts all of the monocarbonyl back to the dicarbonyl species. Attempts to remove the final CO ligand have been attempted by both photochemical and thermal routes, but it does not appear to be labile even under forcing conditions.

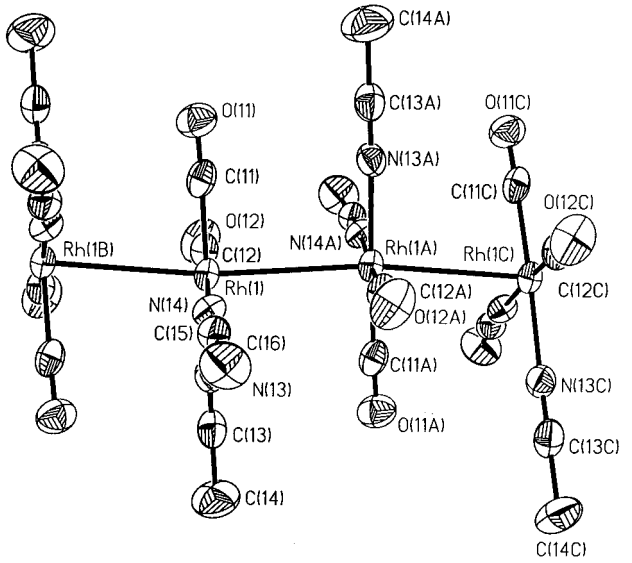

Figure 13. A 50% thermal ellipsoid plot for a tetrameric segment of the cation stacks in $[Rh(CO)_2(MeCN)_2][BF_4]$, **6**. The tetrafluoroborate anions have been removed for clarity.

3. Crystal Structure. Although the cation $[Rh(MeCN)_2(CO)_2]^+$ has been crystallized in other salts, this is the first instance in which the cation has a dominant role in the packing.[37b,c] In earlier structures, the anions were bulky rhodium carbonyl/carbide clusters that defined the dimensions of the unit cell and also dictated the connectivity of the $[Rh(MeCN)_2(CO)_2]^+$ units. As Figure 13 shows, the rhodium cations form an extended chain consisting of 3.1528(14) and 3.1811(14) Rh−Rh contacts. These distances are slightly shorter than the "dimer" stacking distance of 3.27 Å described by Albano and co-workers for the cations in $[Rh(MeCN)_2(CO)_2]_2[Rh_{14}C_2(\mu\text{-}CO)_{21}(CO)_{12}]$.[37c] Obviously the smaller $[BF_4]^-$ anions allow for closer association of Rh^I ions into 1-D stacks, a situation that has been recognized for square-planar Rh(I) molecules with sterically undemanding ligands.[36]

IV. Conclusions

Salts of the singly bonded cation $[Rh_2(MeCN)_{10}]^{4+}$ provide the basis for the new chemistry of rhodium, an extremely important element in coordination and organometallic chemistry. These compounds are highly unusual in that they span several oxidation states, yet they are all stabilized by only MeCN ligands. The presence of labile nitriles allows the cations to be introduced into a variety of settings under mild conditions. Convenient, nonaqueous routes have been developed to access homoleptic dinuclear MeCN complexes of Rh; these can easily be tailored for extension to other nitriles such as propionitrile as demonstrated by the synthesis of $[Rh_2(EtCN)_{10}]^{4+}$. The redox properties of $[Rh_2(MeCN)_{10}]^{4+}$ were probed both electrochemically and chemically, investigations that led to the realization that both oxidized and reduced forms of $Rh_2^{II,II}$ could be prepared. The oxidized, mononuclear compound $[Rh^{III}(MeCN)_6][BF_4]_3$ (**4**) and the reduced, polymeric material $[Rh^{I,II}(MeCN)_4(BF_4)_{1.5}]_x$ (**5**) were crystallized and their properties investigated. $[Rh(CO)_2(MeCN)_2][BF_4]$ (**6**), which converts to $[Rh(CO)(MeCN)_3][BF_4]$ in solution, was crystallized and found to contain a weakly interacting 1-D chain of Rh^I cations. Facile replacement of MeCN ligands with other RCN donors should be possible for the labile d^8 Rh^I centers, which adds even more flexibility to the chemistry of the homologous series. In short, $[Rh_2(MeCN)_{10}][BF_4]_4$ has provided an entry into a series of

(34) (a) Coulon C. *Organic and Inorganic Low Dimensional Crystalline Materials*; Delhaes, P., Drillon, M., Eds.; NATO ASI Series B; Plenum Press: New York, 1987; p 201. (b) Dumoulin, B.; Bourbonnais, C.; Ravy, S.; Pouget, J. P.; Coulon, C. *Phys. Rev. Lett.* **1996**, *76*, 1360.

(35) (a) Ugo, R.; Bonati, F.; Fiore, M. *Inorg. Chim. Acta* **1968**, *2*, 463. (b) Epstein, R. A.; Geoffrey, G. L.; Keeney, M. E.; Mason, W. R. *Inorg. Chem.* **1979**, *18*, 478.

(36) (a) Mann, K. R.; DiPerro, M. J.; Gill, T. P. *J. Am. Chem. Soc.* **1980**, *102*, 3965.

(37) (a). Brown, C.; Heaton, B. T.; Longhetti, L.; Povey, W. T.; Smith, D. O. *J. Organomet. Chem.* **1980**, *192*, 93. (b) Albano, V. G.; Chini, P.; Martinengo, S.; Sansoni, M.; Strumolo, D. *J. Chem. Soc., Chem. Commun.* **1974**, 299. (c) Martinengo, S.; Strumolo, D.; Chini, P.; Albano, V. G.; Braga, D. *J. Chem. Soc., Dalton Trans.* **1984**, 1837.

solvated ions of Rh in various oxidation states that exhibit a range of properties both in solution and in the solid state. It is quite remarkable that one ligand can allow for such a rich series of homoleptic complexes to be accessed.

Acknowledgment. The authors acknowledge Johnson-Matthey for a loan of rhodium trichloride and the National Science Foundation for support of this work (NSF CHE-9622589). We also acknowledge the assistance of Dr. Donald Ward and Xiang Ouyang for advice on crystallography, and Prof. Eugenio Coronado and Dr. Carlos Goméz-Garcia for assistance with the magnetic susceptibility study. The authors thank Patrick Batail for useful comments and the financial support of DGES-Spain (Project PB96-0859) to E.C. Partial financial support for L.E.P. was obtained from Dow Chemical and Michigan State University College of Natural Science.

Supporting Information Available: Additional information for $[Rh_2(MeCN)_{10}][BF_4]_4$, $[Rh_2(MeCN)_{10}][O_3SCF_3]_4$, $[Rh_2(EtCN)_{10}][BF_4]_4$, $[Rh(MeCN)_6][BF_4]_3$, $\{[Rh_2(MeCN)_4][BF_4]_{1.5}\}_x$, and $[Rh(MeCN)_2(CO_2)][BF_4]$ (PDF). This material is available free of charge via the Internet at http://pubs.acs.org.

JA991130E